Biol. Cybern. 67, 133–141 (1992)

Biological Cybernetics

A general diffusion model for analyzing the efficacy of synaptic input to threshold neurons

G. T. Kenyon [1], R. D. Puff [2], and E. E. Fetz [3]

[1] Division of Neuroscience, Baylor College of Medicine, Houston, TX 77030, USA
[2] Department of Physics FM-15, University of Washington, Seattle, WA 98195, USA
[3] Department of Physiology and Biophysics SJ-40, University of Washington, Seattle, WA 98195, USA

Received May 21, 1991/Accepted February 4, 1992

Abstract. We describe a general diffusion model for analyzing the efficacy of individual synaptic inputs to threshold neurons. A formal expression is obtained for the system propagator which, when given an arbitrary initial state for the cell, yields the conditional probability distribution for the state at all later times. The propagator for a cell with a finite threshold is written as a series expansion, such that each term in the series depends only on the infinite threshold propagator, which in the diffusion limit reduces to a Gaussian form. This procedure admits a graphical representation in terms of an infinite sequence of diagrams. To connect the theory to experiment, we construct an analytical expression for the primary correlation kernel (PCK) which profiles the change in the instantaneous firing rate produced by a single postsynaptic potential (PSP). Explicit solutions are obtained in the diffusion limit to first order in perturbation theory. Our approximate expression resembles the PCK obtained by computer simulation, with the accuracy depending strongly on the mode of firing. The theory is most accurate when the synaptic input drives the membrane potential to a mean level more than one standard deviation below the firing threshold, making such cells highly sensitive to synchronous synaptic input.

1 Introduction

The present investigation aims toward a mathematical description of nervous system activity that captures interesting dynamical behaviors and yet remains amenable to analytical techniques. Specifically, we present a novel solution to a general diffusion model which adequately describes the synaptic interactions between biological nerve cells. The time-dependent perturbation methods employed here are a generalization of techniques previously described (Cowan 1972). In this preliminary investigation we have limited our analysis to the effects of synaptic input on the firing activity of a single cell. However, the computational procedure described here is quite general and may be readily extended to the analysis of interacting neural systems.

To assess the accuracy of our computational procedure, the model is used to predict the efficacy of individual synaptic inputs under various dynamical conditions. This is accomplished by deriving an explicit expression for the primary correlation kernel (PCK) (Knox 1974), which profiles the change in the instantaneous firing rate produced by a synaptic impulse, or postsynaptic potential (PSP). The synaptic efficacy, A, is then defined as the total area under the PCK and yields the average number of additional (or missing) firings associated with the PSP. For comparison, the actual PCK is then estimated from computer simulated spike train data. In the present study, we only consider synaptic input that is Poisson-distributed, which eliminates all secondary effects due to the autocorrelation of the presynaptic source (Moore et al. 1970).

Attempts to quantify the relationship between the PSP and the PCK have been made by several investigators (Knox 1974; Kirkwood and Sears 1978; Fetz and Gustafsson 1983). Knox (1974) examined both the primary and secondary components found in the cross-correlation of two spike trains but only obtained explicit solutions for the PCK produced by excitatory PSPs (EPSPs) with infinitesimally short rise times ("first-order" EPSPs). Instantaneous rise times are not physiologically realistic, however, and introduce abnormal firing properties since threshold crossings are restricted to the initial depolarizing jump. Kirkwood and Sears (1978), on the basis of indirect empirical observations, proposed that the PCK is proportional to both the PSP and its first time derivative. Fetz and Gustafsson (1983) derived a linear relationship from a study of motor neurons using a threshold crossing model with a smooth linear ramp to threshold. Their analysis was later corroborated by a physiological study of the PCK produced by single 1a afferent fibers on motor neurons (Cope et al. 1987). We know from both numerical and

Correspondence to: G. T. Kenyon

mathematical analysis, however, that in the general case the relation between the PCK and the PSP is more complicated, although the linear approximation may be valuable for estimating the effects of network connectivity on pairwise firing correlations in certain dynamical regimes (Kenyon et al. 1990; Fetz 1988).

Another relevant line of research involves the modeling of cell firing activity as the consequence of a diffusion process (cf. Gerstein and Mandelbrot 1964; Johannesma 1968; Holden 1976; Sampath and Srinivassan 1977; Giorno et al. 1988). These investigations have been principally directed toward solving the first passage time problem and thereby obtaining the average firing rate as a function of the parameters characterizing the synaptic input. These models have also been extended to analyze both the dynamics of large networks and the transient responses produced by synaptic inputs (Brannan and Boyce 1981a, b). The analytical methods developed in these studies are limited, however, to the consideration of synaptic inputs of either zeroth order (perfect integrator) or first order form (leaky integrator).

All of the above models possess some region of validity, but none are generally applicable over a wide range of dynamical conditions. The theoretical model presented here is a first attempt at a unified treatment of the response properties of single cells that may be readily extended to the analysis of larger interacting systems. Our immediate goal is to predict the time-dependent changes in the instantaneous firing rate produced by typical synaptic inputs. We further seek to understand how such changes depend on dynamical factors, such as the intensity and character of the background synaptic input.

In Sects. 2 and 3 we describe both our analytical model and the numerical methods used to generate spike train data. In Sect. 4, the analytical and simulated results are compared. Finally, in Sect. 5, we discuss the dynamical factors affecting the relationship between the PCK and the PSP. We also consider both the strengths and weaknesses of the calculational procedure outlined here, as well as indicating how the present model may be extended to more accurately reflect physiological nerve cells.

2 Analytical methods

2.1 Threshold neuron models

The neuron model considered here, called an integrate-and-fire model in the literature, is conceptually simple. The neuron sums Poisson-distributed PSPs representing the synaptic input from a large presynaptic population of cells. When the combined synaptic input exceeds a threshold value, the neuron 'fires' and the membrane potential is reset. In the simplest version of the model, we assume that all synapses produce PSPs of identical size and shape, which we take to be of second order form (i.e. the sum of two exponential decays). The process may then be written compactly in terms of a second-order differential equation with an additional threshold firing condition:

$$\left(\tau_r \frac{\partial^2}{\partial t^2} + \frac{\partial}{\partial t} + \frac{1}{\tau_d}\right) \phi(t) = \sum_{t'} T\delta(t - t') \,. \tag{1}$$

The left hand side of (1) consists of an ordinary, linear differential operator acting on the membrane polarization at time t, $\phi(t)$. Individual PSPs are generated by each δ-function impulse, where the impulse amplitude is given by T and the sum is over the arrival times of all inputs. τ_r and τ_d give the rise and decay times of the PSP, respectively.

The threshold firing condition is given by

$$\text{if} \quad \phi(t) = \theta \quad \text{then} \quad \begin{matrix} \phi(t + 0^+) \to \phi_r \\ \dot{\phi}(t + 0^+) \to \dot{\phi}_r \end{matrix} \tag{2}$$

where θ is the firing threshold. After firing, the state of the neuron is reset according to the fixed 'reset' potentials $\{\phi_r, \dot{\phi}_r\}$ and we require that $\phi_r < \theta$.

It is convenient to rewrite (1) in the following form:

$$\frac{\partial}{\partial t} \boldsymbol{\phi}(t) + \overleftrightarrow{\Gamma} \cdot \boldsymbol{\phi}(t) = \sum_{t'} \mathbf{T}\delta(t - t') \tag{3}$$

where we have introduced the vector notation for the membrane polarization and its first time derivative, $\boldsymbol{\phi} = (\phi, \dot{\phi})^T$.

Comparing (1) and (3), we see that the components of the drift matrix, $\overleftrightarrow{\Gamma}$ in the 2×2-dimensional space are given by

$$\overleftrightarrow{\Gamma} = \begin{pmatrix} 0 & -1 \\ \dfrac{1}{\tau_r \tau_d} & \dfrac{1}{\tau_r} \end{pmatrix} \tag{4}$$

and that the impulse strength, T, has been generalized to a 2-dimensional vector with components $\mathbf{T} = (0, T/\tau_r)^T$.

2.2 The infinite threshold propagator

Consider a neuron with an infinite firing threshold bombarded by Poisson-distributed impulses arriving at a mean frequency f. The statistical distribution of the membrane polarization is governed by a generalized Fokker–Planck equation of the form

$$\frac{\partial}{\partial t} G^{(\infty)}(\boldsymbol{\phi}, t|\boldsymbol{\phi}', \mathbf{t}) = \delta(t - t')\delta(\boldsymbol{\phi} - \boldsymbol{\phi}') + \left\{\frac{\partial}{\partial \boldsymbol{\phi}} \cdot \overleftrightarrow{\Gamma} \cdot \boldsymbol{\phi} + f\left[\exp\left\{-\mathbf{T} \cdot \frac{\partial}{\partial \boldsymbol{\phi}}\right\} - 1\right]\right\} \times G^{(\infty)}(\boldsymbol{\phi}, t|\boldsymbol{\phi}', t') \,. \tag{5}$$

$G^{(\infty)}(\boldsymbol{\phi}, t|\boldsymbol{\phi}', t')$ is the propagator for the infinite threshold neuron, which gives the probability density for finding the cell in the state $\boldsymbol{\phi}$ at time t, given the cell was in state $\boldsymbol{\phi}'$, at the earlier time, t'. The derivation of (5) depends only on the general form of (3) and on the condition that the synaptic input be Poisson-distributed (Gardiner 1983).

2.3 The diffusion limit

We are most interested in the solution to (5) in the diffusion or low noise limit. Expanding the translation operator, also called the 'jump term', as a power series in T, and then neglecting all terms of order $O(T^3)$ and above, we obtain a Fokker–Planck equation of the form

$$\frac{\partial}{\partial t}G^{(\infty)}(\boldsymbol{\phi}, t|\boldsymbol{\phi}', t') = \delta(t-t')\delta(\boldsymbol{\phi}-\boldsymbol{\phi}') + \left\{\frac{\partial}{\partial \boldsymbol{\phi}}\cdot(\overleftrightarrow{\Gamma}\cdot\boldsymbol{\phi} - f\mathbf{T}) + \frac{1}{2}\mathrm{Tr}\left[\left(\frac{\partial}{\partial\boldsymbol{\phi}}\otimes\frac{\partial}{\partial\boldsymbol{\phi}}\right)\cdot\overleftrightarrow{\Sigma}\right]\right\} \times G^{(\infty)}(\boldsymbol{\phi}, t|\boldsymbol{\phi}', t') . \quad (6)$$

where we have introduced the (2×2) diffusion matrix $\overleftrightarrow{\Sigma}$, given by

$$\overleftrightarrow{\Sigma} = f\mathbf{T}\otimes\mathbf{T} . \quad (7)$$

We see that the diffusion, or low noise, approximation becomes exact in the limit $f\to\infty$ and $T\to 0$ such that the product fT remains finite.

In the diffusion limit, the infinite threshold propagator, $G^{(\infty)}$, is a two dimensional Gaussian distribution:

$$G^{(\infty)}(\boldsymbol{\phi}, t|\boldsymbol{\phi}', t') = \frac{\exp\{-\frac{1}{2}(\boldsymbol{\phi}-\langle\boldsymbol{\phi}(t-t')\rangle)^T\cdot\overleftrightarrow{\sigma}^{-1}(t-t')\cdot(\boldsymbol{\phi}-\langle\boldsymbol{\phi}(t-t')\rangle)\}}{2\pi\sqrt{\|\overleftrightarrow{\sigma}(t-t')\|}} \quad (8)$$

such that $G^{(\infty)}$ is completely determined by the first two cumulants of the distribution, $\langle\boldsymbol{\phi}(t-t')\rangle$ and $\overleftrightarrow{\sigma}(t-t')$. From (6) we may derive formal solutions for the first two cumulants:

$$\langle\boldsymbol{\phi}(t-t')\rangle = \mathrm{e}^{(t-t')\overleftrightarrow{\Gamma}}\cdot(\boldsymbol{\phi}'-\langle\boldsymbol{\phi}(\infty)\rangle)+\langle\boldsymbol{\phi}(\infty)\rangle \quad (9)$$

$$\overleftrightarrow{\sigma}(t-t') = -\mathrm{e}^{(t-t')\overleftrightarrow{\Gamma}}\cdot\overleftrightarrow{\sigma}(\infty)\cdot\mathrm{e}^{(t-t')\overleftrightarrow{\Gamma}^T}+\overleftrightarrow{\sigma}(\infty) \quad (10)$$

Finally, a similar calculation shows that the stationary values of the first two cumulants are given by

$$\langle\boldsymbol{\phi}(\infty)\rangle = \tau_d f T\begin{pmatrix}1\\0\end{pmatrix} \quad (11)$$

$$\overleftrightarrow{\sigma}(\infty) = \tfrac{1}{2}\tau_d f T^2\begin{pmatrix}1 & 0\\ 0 & \dfrac{1}{\tau_r\tau_d}\end{pmatrix} . \quad (12)$$

Equations (8)–(12) provide an explicit solution for the infinite threshold propagator in the diffusion limit. It will be useful for the following development, however, to rewrite (6) in terms of the inverse propagator:

$$\int_{-\infty}^{\infty}\mathrm{d}t''\int_{-\infty}^{\infty}\mathrm{d}\boldsymbol{\phi}''G^{(\infty)-1}(\boldsymbol{\phi}, t|\boldsymbol{\phi}'', t'')\times G^{(\infty)}(\boldsymbol{\phi}'', t''|\boldsymbol{\phi}', t') = \delta(t-t')\delta(\boldsymbol{\phi}-\boldsymbol{\phi}') \quad (13)$$

with the inverse of $G^{(\infty)}$ given formally by

$$G^{(\infty)-1}(\boldsymbol{\phi}, t|\boldsymbol{\phi}, t') = \left\{\frac{\partial}{\partial t} - \left\{\frac{\partial}{\partial\boldsymbol{\phi}}\cdot(\overleftrightarrow{\Gamma}'\boldsymbol{\phi} - f\mathbf{T}) + \frac{1}{2}\mathrm{Tr}\left[\left(\frac{\partial}{\partial\boldsymbol{\phi}}\otimes\frac{\partial}{\partial\boldsymbol{\phi}}\right)\cdot\overleftrightarrow{\Sigma}\right]\right\}\right\} \times\delta(t-t')\delta(\boldsymbol{\phi}-\boldsymbol{\phi}') . \quad (14)$$

2.4 The finite threshold propagator

It now remains to obtain an expression for the full propagator, G. We do this by appending probability current sources and sinks to the Fokker–Planck equation.

A probability current sink, J_-, acting at the firing threshold is defined by

$$J_-(\boldsymbol{\phi}, t|\boldsymbol{\phi}, t') = -\delta(\phi-\theta)[\dot{\phi}]G(\boldsymbol{\phi}, t|\boldsymbol{\phi}', t') \quad (15)$$

J_- gives the rate at which probability flows out of the subthreshold region with a given $\dot{\phi}$ for a cell prepared in state $\boldsymbol{\phi}'$ at time t'. The form of the expression for the current (15) may be understood by noting that it is just the product of a probability density, G, with a 'normal velocity', $\dot{\phi}$. The extra δ-function factor simply localizes the probability current sink at the firing threshold.

A probability current source, J_+, acting at the reset potentials, $\boldsymbol{\phi}_r$, is likewise given by

$$J_+(\boldsymbol{\phi}, t|\boldsymbol{\phi}', t') = \delta(\boldsymbol{\phi}-\boldsymbol{\phi}_r)\int_0^{\infty}\mathrm{d}\dot{\phi}[\dot{\phi}'']G(\boldsymbol{\theta}'', t|\boldsymbol{\phi}', t') \quad (16)$$

where we have introduced the vector $\boldsymbol{\theta}$ with components $\boldsymbol{\theta} = (\theta, \dot{\phi})^T$. J_+ gives the rate at which probability flows into the system at the reset potentials, $\boldsymbol{\phi}_r$.

The total integral over the 2-dimensional phase space is the same for both currents:

$$\int_{-\infty}^{\infty}\mathrm{d}\boldsymbol{\phi}J_-(\boldsymbol{\phi}, t|\boldsymbol{\phi}', t') = \int_{-\infty}^{\infty}\mathrm{d}\boldsymbol{\phi}J_+(\boldsymbol{\phi}, t|\boldsymbol{\phi}', t') \quad (17)$$

as is required by current conservation. Any probability current that leaves at the threshold must come back in at the reset potentials.

These current sources and sinks are then appended to the right hand side of (13) to yield an integral equation for the finite threshold propagator, G. Multiplying through by $G^{(\infty)}$ and integrating over all intermediate states then results in the following Dyson equation:

$$G(\boldsymbol{\phi}, t|\boldsymbol{\phi}', t) = G^{(\infty)}(\boldsymbol{\phi}, t|\boldsymbol{\phi}', t') + \int_{t'}^{t}\mathrm{d}t''\int_{-\infty}^{\infty}\mathrm{d}\boldsymbol{\phi}G^{(\infty)}(\boldsymbol{\phi}, t|\boldsymbol{\phi}'', t'')\{J_+(\boldsymbol{\phi}'', t''|\boldsymbol{\phi}', t') - J_-(\boldsymbol{\phi}'', t''|\boldsymbol{\phi}', t')\}. \quad (18)$$

Substituting the explicit forms for J_+ (16) and J_- (15) we obtain

$$G(\boldsymbol{\phi}, t|\boldsymbol{\phi}', t') = G^{(\infty)}(\boldsymbol{\phi}, t|\boldsymbol{\phi}', t') + \int_{t'}^{t}\mathrm{d}t''\int_0^{\infty}\mathrm{d}\dot{\phi}'' \times\{G^{(\infty)}(\boldsymbol{\phi}, t|\boldsymbol{\phi}_r, t'') - G^{(\infty)}(\boldsymbol{\phi}, t|\boldsymbol{\theta}'', t'')\}[\dot{\phi}'']G(\boldsymbol{\theta}'', t''|\boldsymbol{\phi}', t') \quad (19)$$

Equation (19) is the principal relation between the finite and infinite threshold propagators and will be our starting point for obtaining approximate solutions.

Examination of (19) shows that G is normalized and satisfies the correct initial conditions as $t \to t'$.

$$\lim_{t \to t'} G(\phi, t|\phi', t') = \delta(\phi - \phi') \tag{20}$$

G must also satisfy the following boundary conditions at the threshold:

$$\begin{aligned} G(\theta, t|\phi', t') &= 0 \quad \text{for} \quad \dot{\phi} < 0 \\ G(\phi, t|\theta', t') &= 0 \quad \text{for} \quad \dot{\phi}' > 0 \end{aligned} \tag{21}$$

These boundary conditions merely specify that no trajectories can enter the allowed subthreshold region from the forbidden region above the threshold.

2.5 Time dependent perturbation theory

Equation (19) may be solved approximately by iterating the expression to the desired order. To zeroth order we have simply:

$$G_{(0)}(\phi, t|\phi', t') = G^{(\infty)}(\phi, t|\phi', t') \tag{22}$$

To first order, we replace G on the right hand side of (19) with $G^{(\infty)}$:

$$\begin{aligned} G_{(1)}(\phi, t|\phi', t') &= G^{(\infty)}(\phi, t|\phi', t') \\ &+ \int_{t'}^{t} dt'' \int_{0}^{\infty} d\phi''\{G^{(\infty)}(\phi, t|\phi_r, t'') \\ &- G^{(\infty)}(\phi, t|\theta'', t'')\}[\dot{\phi}'']G^{(\infty)}(\theta'', t''|\phi', t'). \end{aligned} \tag{23}$$

2.6 Graphical representation

Consistent with a path integral representation, the propagator between two states is formally equal to the weighted sum of all possible trajectories between the two states. Equation (22) shows that to lowest order G is given by the weighted sum of all trajectories in the source/sink free system. In (19), the sink term removes all trajectories which previously crossed the threshold. The source term adds these trajectories back in at the appropriate reset potentials.

In Fig. 1 we present a graphical representation of the above procedure. The curves on each graph refer to the associated propagator between the two states at two indicated times. The thick curves represent the finite threshold propagator G, and the thin curves stand for the infinite threshold propagator, $G^{(\infty)}$. Each vertex, shown in Fig. 1 as large round dots, implies an integration over all intermediate times and states. A vertex at a threshold crossing carries an additional δ-function which forces the membrane and threshold potentials to be equal. Likewise, a vertex at the reset potential carries two δ-functions. Of course, the states represented on the graphs are actually 2-dimensional, but only one dimension is necessary to illustrate the procedure. It is thus possible to formulate a complete set of rules such that both the graphical and algebraic representations contain the same information. Such graphical representations are useful for both organizing and clarifying complex mathematical expressions.

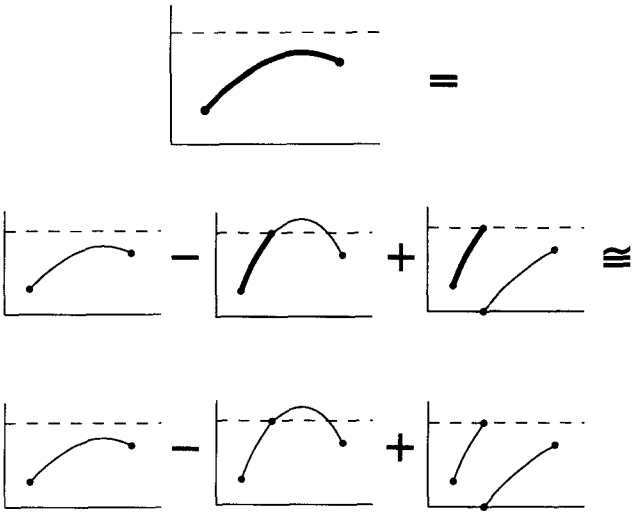

Fig. 1. Graphical representation of perturbation calculation. The first equality gives the exact relation (19) between the finite and infinite threshold propagators. The second equality exhibits the first two terms in the perturbation series (23) obtained by iteratively replacing the finite threshold propagator with its formal expansion and then neglecting all graphs with more than one vertex. Each vertex implies integration over all intermediate times and over all non fixed membrane potential degrees of freedom. The graphical representation contains the same information as the explicit algebraic form, but is conceptually simpler. ———, finite threshold propagator; ———, infinite threshold propagator

The first equality in Fig. 1, which corresponds to (19), portrays the exact relationship between the finite and infinite threshold propagators. The second equality corresponds to (23) and exhibits the first two terms in the perturbation series. In general, we see that the finite threshold propagator is constructed from the infinite threshold propagator by subtracting all 'illegal' suprathreshold trajectories and adding back in the correctly 'reset' trajectories. Consecutive terms in the perturbation series are obtained simply by iteratively replacing the finite threshold propagator by the expansion shown in the first equality in Fig. 1 and then neglecting all graphs above a certain order, determined by the number of vertices.

2.7 Experimental measures

The firing rate of the cell is equal to the probability current flowing out through the boundary at $\phi = \theta$ where (15) gives the general form for this current:

$$\begin{aligned} F(t|\phi', t') &= \int_{0}^{\infty} d\dot{\phi} J_{-}(\theta, t|\phi', t'). \\ &= \int_{0}^{\infty} d\dot{\phi}[\dot{\phi}]G(\theta, t|\phi', t'). \end{aligned} \tag{24}$$

The stationary firing rate is then found by letting $t - t' \to \infty$:

$$F(\infty) = \int_{0}^{\infty} d\dot{\phi}[\dot{\phi}]G(\theta, \infty). \tag{25}$$

The PCK, denoted by $C(t - t')$, produced by an impulse of strength S delivered to a cell in the station-

ary state at time t' is given by

$$C(t-t') = \int_0^\infty d\phi \int_{-\infty}^\infty d\phi' \, d\dot{\phi}'[\dot{\phi}] \times G(\boldsymbol{\theta}, t|\boldsymbol{\phi}' + \mathbf{S}, t')G(\boldsymbol{\phi}, \infty) \quad (26)$$

where $\mathbf{S} = (0, S)^T$. We have used the fact that the effect of an impulse of amplitude S delivered to a system governed by equation 1 is to modify $\langle \boldsymbol{\phi}(t-t') \rangle$ by shifting the initial conditions; $\boldsymbol{\phi}' \to \boldsymbol{\phi}' + \mathbf{S}$.

Equation (26), giving the primary correlation kernel produced by an impulse of strength S, may be compared to a similar expression obtained by Knox (1974). The difference in the two expressions is that we have assumed an underlying Markov process which allows us to integrate over a complete set of states at the time the impulse is applied.

2.8 Solutions for the PCK up to first order

Expressions for the PCK of successively greater accuracy are obtained by first expanding G and then inserting the results in (26) for the PCK where all terms above the desired order are neglected. To zeroth order, we have therefore

$$C_{(0)}(t-t') = \int_0^\infty d\phi \int_{-\infty}^\infty d\phi' \int_0^\infty d\dot{\phi}'[\dot{\phi}] \times G^{(\infty)}(\boldsymbol{\theta}, t|\boldsymbol{\phi}' + \mathbf{S}, t')G^{(\infty)}(\boldsymbol{\phi}', \infty) \quad (27)$$

To obtain an expression accurate to first order, we note the property of Gaussian distributions that the convolution of two Gaussians is another Gaussian:

$$\int_{-\infty}^\infty d\boldsymbol{\phi}' G^{(\infty)}(\boldsymbol{\phi}, t|\boldsymbol{\phi}' - \mathbf{S}, t')G^{(\infty)}(\boldsymbol{\phi}', t'|\boldsymbol{\phi}'', t'') = G^{(\infty)}(\boldsymbol{\phi} - \mathbf{e}(t-t'), t|\boldsymbol{\phi}'', t'') \quad (28)$$

where we have written the impulse response function (PSP) as $e(t-t')$ and we have adopted the shorthand notation $\mathbf{e}$ for $\{e, \dot{e}\}$. We then obtain to first order for the PCK

$$\begin{aligned} C_{(1)}(t-t') = C_{(0)}(t-t') + \int_{-\infty}^t dt'' \int_0^\infty d\dot{\phi} \int_0^\infty d\dot{\phi}'' \\ \times \{[\dot{\phi}]G^{(\infty)}(\boldsymbol{\theta} - H(t'-t'')\mathbf{e}(t-t'), t|\boldsymbol{\phi}_r, t'')[\dot{\phi}'']] \\ \times G^{(\infty)}(\boldsymbol{\theta}'' - \mathbf{e}(t''-t'), \infty) - [\dot{\phi}]G^{(\infty)}(\boldsymbol{\theta} - H(t'-t'') \\ \times \mathbf{e}(t-t'), t|\boldsymbol{\theta}'', t'')[\dot{\phi}'']G^{(\infty)}(\boldsymbol{\theta}'' - \mathbf{e}(t''-t'), \infty)\} \end{aligned} \quad (29)$$

where we have introduced the step function $H(x)$ which is unity for $x > 0$ and zero otherwise. We have also adopted the convention that $C_{(1)}(t-t')$ denotes the PCK obtained by neglecting all graphs with more than one vertex.

Equation (29) gives our approximate expression for the PCK valid to first order in the perturbation scheme depicted in Fig. 1. It is to our knowledge the first explicit expression for the change in firing rate produced by single synaptic inputs of nonspecific form. All we have left to do is to perform the three remaining integrals in (29), where the integrand consists entirely of known functions. Although conceptually straightforward, the integrals involved are not analytic and therefore cannot be reduced to elementary functions. The details involved in reducing (29) to a more elementary form involving standard error functions have been derived elsewhere (Kenyon 1990).

3 Numerical Methods

3.1 Description of simulation

To test the accuracy of the approximations used in deriving our results, we compared the predictions of the theory to the 'true' PCK calculated from computer generated spike trains obtained by solving (1) and (2) numerically. Due to the linearity of (1), a numerical solution to the dynamical equations may be obtained to an arbitrary degree of precision in continuous time, without introducing an integration time step.

In simulating the activity of threshold neurons, two independent sources of Poisson-distributed synaptic input were employed. The first, or primary source accounted for at least 99% of the total membrane polarization. The secondary source provided a means of testing the response to synaptic impulses of various sizes and never represented more than a small addition to the primary synaptic drive.

When two sources of Poisson-distributed synaptic impulses are present, they may (in the diffusion limit) be replaced by a single equivalent source of synaptic input. The amplitude and frequency of the impulses from the equivalent source are determined by requiring that the first and second moments of the membrane polarization be the same in either case. From (11) and (12) we see this requirement is expressed mathematically as:

$$fT = f_1 T_1 + f_2 T_2 \quad (30)$$

$$fT^2 = f_1 T_1^2 + f_2 T_2^2 \quad (31)$$

where f and T denote the frequency and amplitude of the equivalent source and the subscripts refer to either of the independent sources. We note that (30) may be trivially generalized to account for any number of independent sources. This establishes that the present model is sufficiently general to account for heterogeneous synaptic input as long as all PSPs are characterized by the same set of time constants.

3.2 Simulation parameters

For all the following simulations, τ_r and τ_d are set to 0.2 ms and 1 ms respectively. These times may be shorter than typical biological time constants but have been chosen for convenience. Since the absolute time scale of a computer simulation is arbitrary, all subsequent results with units of time can be scaled accordingly. The ratio $r = \tau_d/\tau_r = 5$ results in EPSPs which are reasonably broad and do not rise too sharply. The reset potentials, ϕ_r and $\dot{\phi}_r$, are 0.0 mV and 0.0 mV/ms respectively. For simplicity, the effects of a postfiring hyperpolarization,which would be indicated by a finite negative value of $\dot{\phi}_r$, was not included in these simulations.

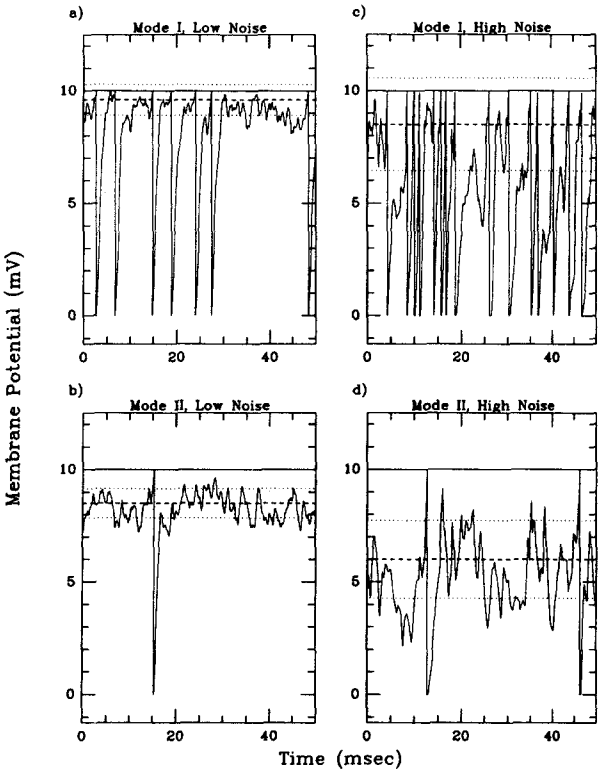

Fig. 2a–d. Example membrane potential trajectories for four different dynamical regimes. Firing mode indicated by individual figure titles. *Dashed line* below threshold indicates the mean asymptotic value (m.a.v.) of the membrane potential in the infinite threshold case. *Dotted lines* indicate one standard deviation above and below the m.a.v. EPSP impulse amplitudes either 1/100 (*low noise*) or 1/10 (*high noise*) of the threshold potential. For activity classified as mode I (mode II), the m.a.v. is (is not) within one standard deviation of the firing threshold

4 Results

4.1 Classifying dynamical regimes

Figure 2 shows four representative membrane potential trajectories, illustrating qualitatively different synaptic input in each case. The firing threshold is indicated by the solid line at 10 mV. The dashed line, computed from (11), indicates the mean asymptotic value (m.a.v.) of the membrane potential. In the absence of a firing threshold, the membrane potential would fluctuate about the m.a.v. The expected amplitude of these fluctuations is given by (12) and is indicated by the two dotted lines which indicate one standard deviation above and below the m.a.v.

Figures 2a, b are labeled low noise since the EPSPs are relatively small ($\theta/100$), and the frequency of incoming EPSP is therefore relatively large (96,000 Hz). In contrast, Figs. 2c, d are labeled high noise since the EPSPs are relatively large ($\theta/10$) and the rate of the Poisson-distributed synaptic input relatively small (8,500 Hz). The relationship between synaptic noise and impulse amplitude follows immediately from (12), which shows that the membrane potential fluctuations increase with the size of the PSPs for fixed m.a.v. Figure 2 shows clearly that the membrane fluctuations are significantly larger in the high noise case.

We also classify the membrane trajectories shown in Fig. 2 by a separate criterion, based on whether or not the m.a.v. of the membrane potential is within one standard deviation of the firing threshold. When the m.a.v. is within one standard deviation of threshold, as in Fig. 2a, c, we classify the resulting firing activity as mode I. Likewise, when the m.a.v. is more than one standard deviation below the firing threshold, as in Fig. 2b, d, we classify the resulting firing activity as mode II. These functional classifications were introduced previously (Kenyon et al. 1990) to characterize the response properties of threshold neurons. In particular, it was shown that the mode of firing activity markedly influenced the effect of firing synchrony on signal propagation (see also Sect. 4.5).

4.2 Stationary firing rates

The stationary firing rates predicted by the theoretical model (25) for each of the four dynamical regimes shown in Fig. 2 are listed in Table 1.

The table reveals that the zeroth order prediction is usually too high and the first order prediction is usually too low. This result is to be expected. To zeroth order the membrane potential is never reset, which causes the firing rate to be overestimated. To first order, the same mechanism causes the theoretical calculation to over count the number of initial threshold crossings and the cell effectively spends too much time in the reset condition, lowering the predicted firing rate below the true value. This pattern of alternately overestimating and then underestimating the true firing rate is repeated to all orders in perturbation theory, ultimately converging on the correct result.

The above arguments are no longer exact when the diffusion approximation is used, since this produces an uncontrolled source of systematic error. However, the diffusion approximation is very good when the PSP amplitudes are small, in which case the above pattern is expected to be a good rule of thumb, if not entirely rigorous. As indicated in Table 1, it is only in the high noise case where diffusion approximation may break down.

Table 1. Stationary firing rates (Hz.): Theory vs. simulation. Firing modes discussed in text and illustrated in Fig. 2. All simulations consisted of approximately 10^5 cell firings (threshold crossings). Theoretical values obtained from 0th and 1st order expansions of (25)

Mode	Simulation ±.5%	Theory	
		0th order	1st order
mode I, low noise	200	301	112
mode II, high noise	24	25	20
mode I, high noise	207	273	160
mode II, high noise	30	25	20

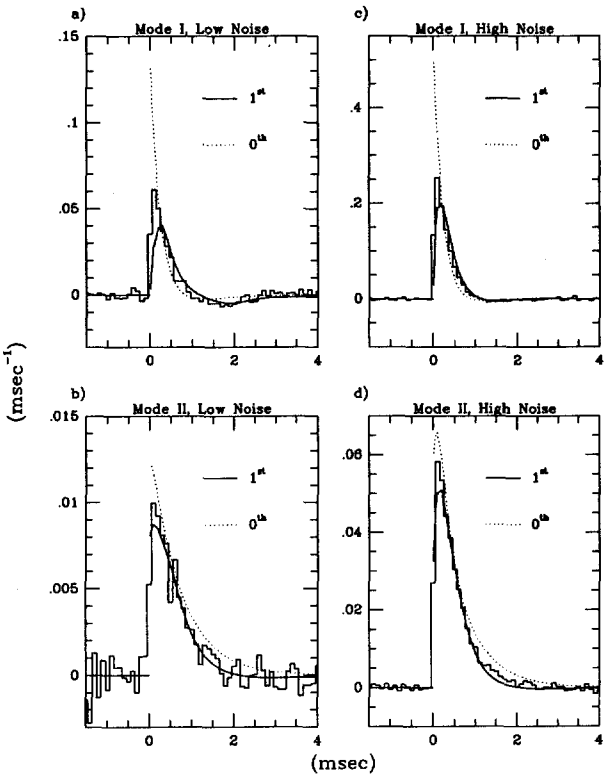

Fig. 3a–d. The PCK produced by an EPSP: Theory vs. Simulation. Comparison of the PCK obtained from simulated spike train data (histogram) with the prediction of a general diffusion model (27, 29) solved to 0th and 1st order in perturbation theory. Data from the four dynamical regimes are organized as in Fig. 2. The theory is a much better fit to the simulation for mode II activity than for mode I activity. The fit is also improved for mode I activity by increasing the level of synaptic noise. The first order correction improves the estimate for PCK in all four dynamical regimes. As predicted, the simulation is usually well bounded by the 0th and 1st order estimates

4.3 The PCK produced by an EPSP

Figure 3 compares the measured PCK produced by a positive synaptic impulse with the two lowest order predictions of the theoretical model. The comparison is made for each of the four dynamical regimes depicted in Fig. 2. For low levels of synaptic noise, the theoretical model predicts the PCK better for mode II than mode I activity. Furthermore, for mode I firing activity, the accuracy of the theoretical model improves with higher levels of synaptic noise, while for mode II activity the effect of increasing noise levels is unclear.

In Fig. 3a the activity is mode I and the membrane fluctuations are relatively small. In this case, the fit between theory and simulation is not very good, although the situation is improved substantially by the first order correction. The discrepancy between theory and simulation is to be expected in this dynamical regime due to the nature of the zeroth order approximation. For mode I activity, the membrane potential crosses the firing threshold fairly often, so the infinite threshold approximation is correspondingly poor. The situation is improved substantially by the first order correction, implying that a higher order calculation would further improve accuracy.

In Fig. 3b, the firing activity is mode II and the membrane fluctuations are again small. In this case, the theory and simulation are in very good agreement. The high degree of accuracy may be anticipated from the nature of the zeroth order approximation and the general validity of the diffusion approximation when applied in this dynamical regime. For mode II activity, threshold crossing are infrequent, and the infinite threshold approximation is reasonably accurate.

In Fig. 3c and d we investigate the effect of increasing levels of synaptic noise on the fit between theory and simulation. For mode I activity (Fig. 3c) the fit is significantly improved by the increased level of synaptic noise. For mode II activity, however (Fig. 3d) no significant effect from increasing noise levels is observed. In the case of mode I activity, increasing the level of synaptic noise makes the infinite threshold approximation more accurate, as the reseting of the membrane potential after each threshold crossing is of the same order of magnitude as the intrinsic membrane fluctuations. In the case of mode II activity, however, the accuracy of the infinite threshold model is not as strongly affected by the level of synaptic noise, since threshold crossing are rare at both noise levels. We still expect, however, that the diffusion approximation is less accurate at higher noise levels, as is evidenced by the fact that the actual firing rate, shown in Table 1, was not within the predicted range for mode II activity at the highest noise level.

4.4 Theoretical bounds on the PCK

Just as the stationary firing rates are bounded by alternating high and low frequency estimates (Table 1) the true PCK should lie between the zeroth and first order results. Thus, even if the PCK is not determined precisely, upper and lower bounds on the PCK may be established. Note that wherever the zeroth and first order results intersect, we obtain an exact value. The same arguments show that more stringent bounds are placed by progressively higher order calculations, such that the first and second order calculations would more effectively bound the true result.

It is apparent from inspection of Fig. 3 that the zeroth and first order predictions do bound the true PCK to within the intrinsic scatter present in the data. The zeroth and first order results are only rigorous bounds in the diffusion limit, however. Again, we must therefore consider the above bounds as a rule of thumb only.

4.5 Synaptic efficacy

We also investigated the PCK as a function of PSP amplitude. We let the synaptic efficacy, A, be defined as the total area under the PCK. A therefore gives the average number of extra spikes produced by the EPSP. Figure 4 shows A as a function of EPSP amplitude for the four distinct dynamical regimes.

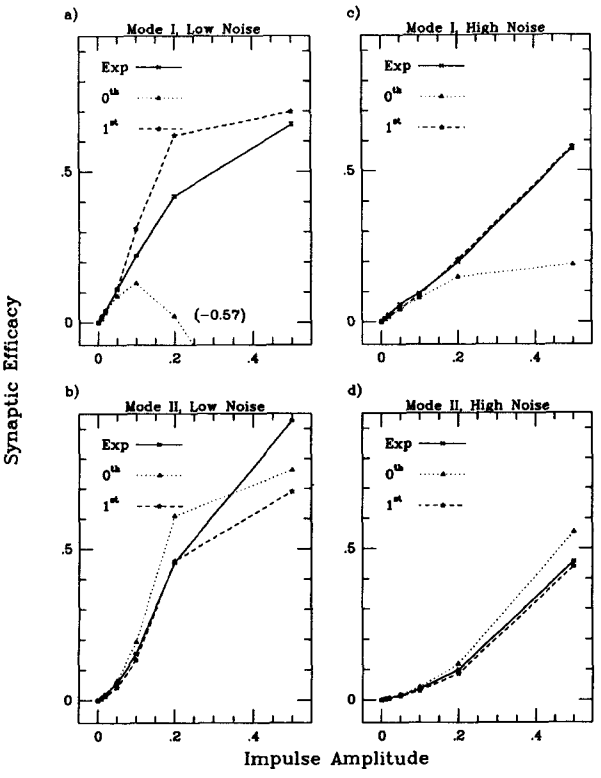

Fig. 4a–d. Synaptic efficacy (Δ) vs. EPSP impulse amplitude: Theory vs. Simulation. Δ obtained by numerically integrating each of the curves in Fig. 3. Δ for large impulses is predicted more accurately in the high noise as opposed to the low noise simulations. As expected, Δ is also more accurately predicted for mode II than for mode I activity. The amplified response to large impulses of neurons with mode II activity is evidenced by the expansive nonlinearity seen in **b** and **d**. In contrast, there is no amplified response to large impulses in cells with mode I activity, as evidenced by the linear or compressively nonlinear relationship seen in **a** and **c**.

Figure 4 reveals a significant functional distinction between mode I and mode II activity. For mode I activity, Δ increases roughly linearly with EPSP size, saturating only for impulse amplitudes greater than 20% of the threshold value in the low noise case. For mode II activity, however, the increase in Δ with EPSP amplitude is non-linear and amplified at large impulse amplitudes, which again, in the low noise case, begins to turn over only at impulse amplitudes above 20% of the firing threshold.

These results imply that cells with mode II activity should be especially sensitive to the synchronous arrival of many EPSPs. It has been shown that this differential sensitivity to synchronous input can be exploited to gate the flow of neurological signals through synaptic pathways (Kenyon et al. 1990). In layered networks, the firing synchrony between cells in a given layer can gate the transmission of frequency modulated signals to subsequent layers. In constrast, there is no corresponding capability in networks with mode I firing activity, since there is no differential selectivity for large inputs. This is evidenced by the initial linear dependence of synaptic efficacy on impulse amplitude for cells with mode I acitivity (Fig. 4a, c).

Figure 4 again shows that to zeroth order, mode II activity is fit much better than mode I activity, although this difference becomes less pronounced when the theory is extended to first order. Figure 4 also confirms our previous observation that synaptic noise improves the fit between theory and experiment for mode I activity, but less so for mode II activity, although the theory is better able to predict the response to very large impulses for either mode of activity when the synaptic noise is also relatively large. It is intuitively reasonable that the theory should describe more accurately the response to synaptic impulses that are of the same order of magnitude as the background synaptic input.

5 Discussion

We have seen that generalized diffusion models can give a good account of the changes in cell firing rate produced by typical synaptic inputs under certain dynamical conditions. Generally, the response of cells exhibiting mode II activity is well described by the theoretical model. This may be of particular significance since mode II firing activity best resembles that observed in cerebral cortex (random, infrequent firings). For cells exhibiting mode I activity, however, the initial terms of the theory are no longer reliable. This may be understood in terms of the method of solution we employed, which uses the results for a cell with an infinite firing threshold to estimate the effects of the finite threshold.

The most important source of the discrepancy between theory and simulation in the mode I case is apparently the assumed form of the zeroth order stationary distribution $G^{(\infty)}(\phi, \infty)$. In the infinite threshold case, the stationary distribution is concentrated at the asymptotic value of the membrane polarization (Fig. 2). When the effect of the finite threshold is included, the probability distribution is spread out due to the resetting of the membrane polarization at each firing. If firings are infrequent, as during mode II activity, this broadening of the distribution is much less substantial and is well estimated to low order. In the mode I case, however, the membrane potential is more likely to be anywhere between the reset polarization and the firing threshold. The best way to improve the theory in the mode I case is therefore to improve the zeroth order estimate of the stationary distribution. We have not yet devised a systematic method for accomplishing this.

It is also possible to understand the qualitative differences in the response to a synaptic impulse exhibited in the two modes of activity. Equation (26) shows that the firing rate is proportional to the time rate of change of the membrane potential at the firing threshold. This is because in a short time interval, Δt, all membrane potential trajectories within $\phi \Delta t$ of the firing threshold will cross the threshold during this interval. One effect of the EPSP is to increase the average time rate of change in the membrane polariza-

tion by an amount $\dot{e}(t-t')$. The EPSP also shifts the distribution of the membrane polarization toward the firing threshold, which also increases the firing rate. In the two modes of activity, these effects have different levels of importance.

In mode I the distribution of the membrane polarization is nearly uniform and therefore relatively independent of the membrane polarization. The effect of the EPSP is then primarily to increase the rate at which membrane potential trajectories cross the firing threshold and the PCK is proportional to $\dot{e}(t-t')$. In mode II the distribution is concentrated at membrane polarizations more than one standard deviation below the firing threshold and the effect of the EPSP is then primarily to shift this distribution closer to the firing threshold. The PCK in the mode II case therefore exhibits a nonlinear dependence of $e(t-t')$ itself.

The generalized diffusion model presented here captures many of the dynamically significant aspects of synaptic interactions between nerve cells. In particular, we are able to reproduce, from a mathematical model, the enhanced sensitivity of neurons with mode II firing activity to large synaptic impulses. This strongly implies that extensions of the formalism to multi-cell networks may be capable of explaining complex behavior involving correlated firing activity.

Finally, we briefly consider several possible generalizations of the above formalism to describe more realistically the synaptic interactions between biological nerve cells. We note that our explicit results are the correct first order expression for a PSP of general shape, given the other assumptions which went into the derivation. Although in the derivation of (29), $e(t-t')$ was assumed to be the response to an impulse of strength S, this was not a requirement, as follows directly from (1).

A finite reversal potential can be incorporated into the formalism by assuming that the amplitude of each synaptic impulse is a function of the membrane polarization. In obtaining a solution for $G^{(\infty)}$, it was necessary to work in the diffusion limit and to assume that the PSP amplitudes were independent of the membrane polarization. To relax these assumptions, a separate perturbation theory would have to be developed for $G^{(\infty)}$. The same techniques used to incorporate the finite threshold into the formalism can also be used to estimate the effects of finite reversal potentials and 'jump' terms neglected in taking the diffusion limit (Kenyon 1990).

Input to biological neurons consists of PSPs that are not only of varying amplitude but of variable time dependence as well. Overdamped second order PSPs with several different time dependences could be included by assuming the total membrane polarization was the sum of several independent membrane polarizations each governed by an equation of the same form as (1), but with different time constants. Spatial interactions between groups of synapses located at different positions along the dendrites could also be modeled in this manner. Likewise, a non-constant threshold could be accounted for by a separate dynamical equation for θ. We have not yet determined how the inclusion of such effects would alter our first order results, but the calculation involved should be straightforward generalization of the steps leading to (29).

Our explicit result for second order PSPs could also be easily extended to PSPs of higher order. The membrane polarization would then be governed by an n^{th} order differential equation where in principle n may be arbitrarily large. This would not alter the form of (29), which is the correct first order expression for the PCK for any theory where the subthreshold membrane polarization obeys a linear differential equation of order greater than 1.

Acknowledgements. The authors wish to thank Dr. David Tam for helpful comments and suggestions. This work was supported by an NIH pre-doctoral training grant in molecular biophysics (grant # T32-GM 08268) and by the Office of Naval Research (contract # N 00018-89-J-1240).

References

Brannan JR, Boyce WE (1981a) Spatially localized interactive neural populations. I. A mathematical model. Bull Math Biol 43:427–446

Brannan JR, Boyce WE (1981b) Spatially localized interactive neural populations. II. Stability and dynamics of excitatory sets. Bull Math Biol 43:427–446

Cope TC, Fetz EE, Matsumura M (1987) Cross-correlation assessment of synaptic strength of single Ia fibre connections with triceps surae motoneurons in cats. J Physiol 390:161–188

Cowan JD (1972) Stochastic models of neuroelectric activity. In: Waddington CH (ed) Towards a Theoretical Biology, vol 4. Aldine, Atherton, pp 169–188

Fetz EE (1988) Correlation strength and computational algebra of synaptic connections between neurons. In: Anderson DZ (ed) Neural Information Processing Systems. American Institute of Physics, pp 270–277

Fetz EE, Gustafsson B (1983) Relation between shapes of post-synaptic potentials and changes in firing probability of cat motoneurones. J Physiol 341:387–410

Gardiner CW (1983) Handbook of Stochastic Methods. Springer Series in Synergetics, vol. 13, 2nd edn. Springer, Berlin Heidelberg New York

Gerstein GL, Mandelbrot B (1964) Random walk models for the spike activity of a single neuron. J Biophys 4:41–67

Giorno V, Lansky P, Nobile AG, Ricciardi LM (1988) Diffusion approximation and first passage time problem for a model neuron. Biol Cybern 58:387–404

Holden AV (1976) Models of the stochastic activity of neurons. Lecture Notes in Biomathematics, vol 12. Springer, Berlin Heidelberg New York

Johannesma PJM (1968) Diffusion models for the stochastic activity of neurons. In: Caianiello ER (ed) Neural networks. Springer, Berlin Heidelberg New York, pp 116–144

Kenyon GT (1990) Mathematical and numerical analysis of firing correlations between nerve cells. PhD thesis, University of Washington, 1990

Kenyon GT, Fetz EE, Puff RD (1990) Effects of firing synchrony on signal propagation in layered networks. In: Touretzky DS (ed) Advances in Neural Information Processing Systems, vol 2. Morgan Kaufmann, San Mateo, Calif., pp 141–148

Kirkwood PA, Sears TA (1978) The synaptic connections to intercostal motoneurons as revealed by the averaged common excitation potential. J Physiol (London) 275:103–134

Knox CK (1974) Cross-correlation functions for a neuronal model. J Biophys 14:567–582.

Moore GP, Segundo JP, Perkel DH, Levitan H (1970) Statistical signs of synaptic interaction in neurons. J Biophys 10:876–900

Sampath G, Srinivasan SK (1977) Stochastic models for spike trains of single neurons. Lecture Notes in Biomathematics, vol 16. Springer, Berlin Heidelberg New York